Structures of Late Transition Metal Monoxides from Jahn-Teller Instabilities in the Rock Salt Lattice

Mariana Derzsi,[1,*] Przemysław Piekarz,[2] and Wojciech Grochala[1]
[1]Centre of New Technologies, The University of Warsaw, Żwirki i Wigury 93, 02079 Warsaw, Poland
[2]Institute of Nuclear Physics, Polish Academy of Sciences, Radzikowskiego 152, 31342 Cracow, Poland
(Received 21 February 2014; revised manuscript received 30 April 2014; published 10 July 2014)

Most late transition metal (LTM) monoxides crystallize in other than a rock salt structure, which is so common in the earlier transition metal monoxides. Here we present theoretical evidence based on density functional theory that an electron-phonon coupling involving a single soft mode in the cubic cell is responsible for the onset of the experimentally observed structures of the late transition metal monoxides.

DOI: 10.1103/PhysRevLett.113.025505 PACS numbers: 61.66.Fn, 61.50.-f, 63.20.dk, 71.70.Ej

Systems containing transition metal (TM) cations are well known for displaying a diversity of phenomena related to the correlated nature of partially occupied d electron states. Distinct variances in the character of an insulating state, magnetic interactions, and charge-orbital ordering observed in these systems reflect a close relationship between the d-state occupancy and electronic properties [1,2]. Since local correlations modify crystal geometry, the interrelation between the electronic and lattice degrees of freedom is a hallmark of TM oxides.

The $3d$ monoxides, MO (M = Ti, V, Cr, Mn, Fe, Co, Ni), represent the best researched group of TM oxides. While they all adopt a simple rock salt structure, some of them exhibit magnetically induced weak rhombohedral [3] or monoclinic distortions [4] at lower temperatures. On the other hand, little is known about the interplay between the electronic and nuclear degrees of freedom in LTM MOs. Among them only NiO, ZnO, and CdO can adopt undistorted rock salt structure, while those containing Cu^{2+}, Pd^{2+}, Pt^{2+}, Hg^{2+}, and mixed valence Ag^{3+}/Ag^{1+} cations crystallize in unique structural types and AuO is unknown. CuO crystallizes in a monoclinic $C2/c$ structure [5]. PdO and PtO both adopt a tetragonal $P4_2/mmc$ [6] structure. AgO crystallizes in two forms, monoclinic $P2_1/c$ [7] and tetragonal $I4_1/a$ [8]. Finally, HgO is known to adopt the orthorhombic $Pnma$ [9], related triclinic $P\bar{1}$ [10], and cinnabar $P3_121$ [11] structure. Considering substantial structural diversity it may be surprising that the crystal structures of LTM MOs can be viewed as distortions of the rock salt lattice. Indeed, it was recently demonstrated that all these compounds adopt quasitetragonally or quasirhombohedrally deformed rock salt superlattices [12] (see Supplemental Material [13] for the rock salt-type representations).

The purpose of this Letter is to provide a unified description of crystal structures of LTM MOs as emerging from the interplay of electronic and nuclear degrees of freedom in the rock salt lattice. Based on the density functional theory (DFT) calculations we will demonstrate that a single phonon mode in the rock salt lattice is responsible for onset of both, the quasi-tetragonal and the quasirhombohedral deformation, while the diversity of the structural types observed among the LTM MOs results due to coupling of additional electronic degrees of freedom to the same lattice mode. This study additionally completes our understanding of crystal structures of all existing TM monoxides as adopting either the perfect or distorted rock salt lattice, the distortion being due to either magnetic ordering or the cooperative Jahn-Teller (JT) effect (Fig. 1).

Orbital ordering in the LTM MOs.— In crystal structures of the LTM MOs, the cations experience either first-order (direct) or second-order (indirect) JT effect, which both lift the degeneracy of the e_g orbitals. The $3d^9$ (Cu^{2+}), $4d^8$ (Pd^{2+}, Ag^{3+}) and $5d^8$ (Pt^{2+}) cations experience direct JT effect—the doubly occupied $d(z^2)$ orbital is stabilized over the empty (for d^8) or half occupied (for d^9) $d(x^2-y^2)$ orbital. In consequence, they are found in a square planar or octahedral coordination. The $4d^{10}$ (Ag^{1+}) and $5d^{10}$ (Hg^{2+}) species experience indirect JT effect—the degeneracy of the e_g orbitals is lifted due to $d(z^2)/s$ mixing, resulting

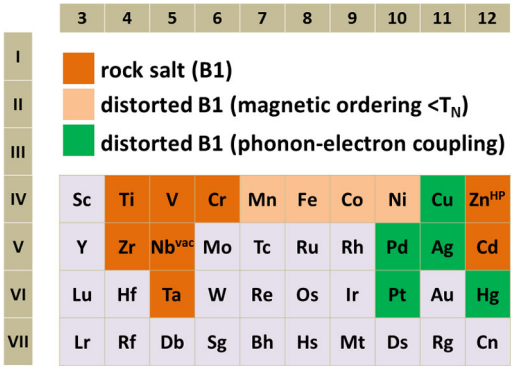

FIG. 1 (color online). The d-block of the Periodic Table of Elements. Transition metal elements which form monoxides, MO, are highlighted orange and green [12,14]. ^{HP} stands for "high pressure" form and ^{vac} for 25% vacancies.

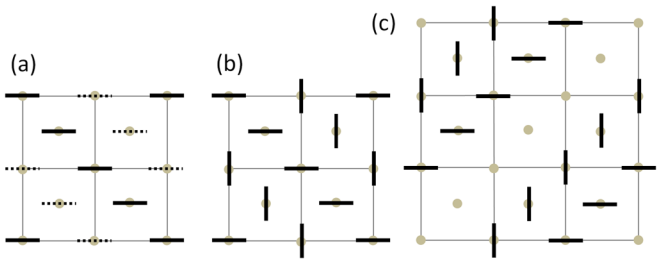

FIG. 2 (color online). Schematic ordering of metal $d(z^2)$ orbitals within a layer of rock salt representations of (a) both forms of AgO ($P2_1/c$ and $I4_1/a$), (b) CuO, PdO, PtO, HgO *Pnma* and HgO $P\bar{1}$, and (c) HgO $P3_121$ (cinnabar). The bold and dotted lines in (a) represent $d(z^2)$ orbitals for contracted Ag^{1+} and elongated Ag^{3+}, respectively. Oxygen atoms are omitted for clarity.

in octahedral contraction (linear coordination). When considering the rock salt-type representations of the LTM MOs [12], the JT-active $d(z^2)$ orbitals follow one of three orbital-ordering patterns: ferrodistortive (FD), anti-FD *ABAB*, or anti-FD *ABC* one (Fig. 2). The FD ordering is observed in both forms of AgO (here the indirect JT effect compensates the direct one), while the *ABAB* pattern is observed in CuO, PdO, PtO and two forms of HgO *Pnma* and $P\bar{1}$. The anti-FD *ABC* ordering pattern is observed only for the cinnabar HgO form.

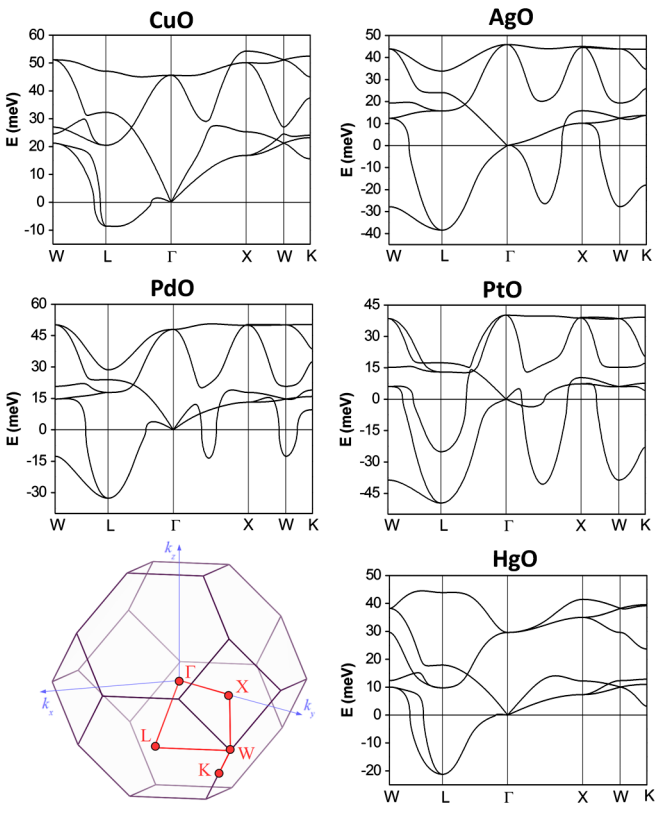

FIG. 3 (color online). Phonon dispersion curves calculated at the DFT (PBEsol) level for the LTM oxides in $Fm\bar{3}m$ cells [15]. Negative energy values represent imaginary frequencies.

Imaginary acoustic phonon.—We have found that all the above-mentioned orbital-ordering patterns couple to a doubly degenerate acoustic mode with the irreducible representation L_3 in the undistorted rock salt structures of respective LTM MOs. This mode, located at the point L (½, ½, ½) in the Brillouin zone, attains the largest imaginary frequency in all cases, while in CuO and HgO it is the only imaginary mode found (Fig. 3). Depending on the number of nonzero components of the order parameter, the L_3 mode reduces the crystal symmetry to different subgroups of the $Fm\bar{3}m$ space group. We consider the deformation with only one nonzero component, which leads to the $C2/c$ monoclinic symmetry and induces atomic distortions predominantly in the oxygen sublattice. It accounts for a substantial reduction of electronic DOS at the Fermi level in CuO, AgO, and PtO and is sufficient enough to open the electronic gap in PdO and

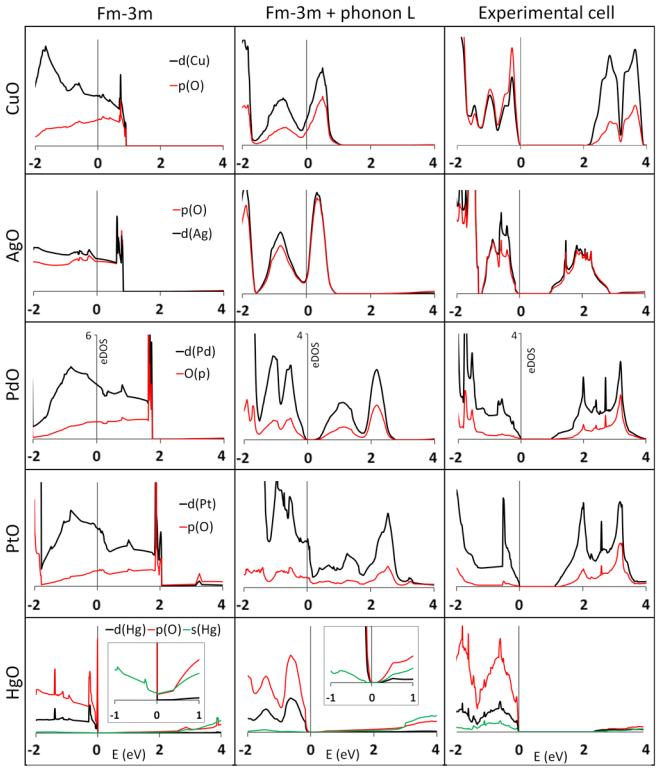

FIG. 4 (color online). Partial electronic DOS (states eV^{-1} $cell^{-1}$) calculated at the hybrid DFT level [16] for the LTM oxides, in hypothetical cubic $Fm\bar{3}m$ cell (left), in modified $Fm\bar{3}m$ cell distorted by the phonon L_3 with no optimization performed (middle) and in the optimized experimentally observed crystal structures (right, spin-polarized calculations were performed for CuO—see text for details). In the case of AgO and HgO, the experimentally observed ground state structures were chosen: AgO $P2_1/c$ and HgO *Pnma*. For t_{2g} and e_g splitting and comparison with DFT(+U) results, see Supplemental Material [13].

HgO (Fig. 4). This indicates a strong coupling between electrons and the soft mode. Metallic character as well as dynamical instability of the LTM MOs in the undistorted cubic cell is obviously due to degeneracy of partially filled and strongly antibonding e_g orbitals of the M^{2+} cations in the octahedral ligand field. In HgO (containing formally closed-shell d^{10} Hg^{2+} cations), the partial depopulation of the e_g orbitals is a consequence of the relativistic low-lying Hg 6s orbitals, which admix to Hg 5d ones (inset in Fig. 4).

Results of the total energy optimization of the imaginary phonon-induced monoclinic structures revealed quasitetragonally distorted rock salt lattice with the anti-FD $ABAB$ ordering [Fig. 2(b)] in all the LTM oxides. In CuO, PdO, AgO, and PtO, where the first-order JT effect took place (octahedral elongation) tetragonal contraction resulted, while in HgO where the second-order JT effect (octahedral contraction) took place tetragonal elongation resulted.

Energetic stabilization of distorted structures.—In the d^8 and d^9 oxides, the orbital ordering enforces additional changes in crystal structures. It is connected with complete removal of the axial ligands from the coordination sphere of the metal cations as the $d(z^2)$ orbitals become substantially stabilized over the $d(x^2-y^2)$ ones. In consequence, the symmetry increases from the monoclinic $C2/c$ ($Z=2$) [17] to its tetragonal supergroup $P4_2/mmc$ ($Z=2$) one. Thus, the $C2/c$ structure plays the role of the *intermediate* phase in the distortion path $Fm\bar{3}m \rightarrow C2/c \rightarrow P4_2/mmc$. In the d^8 oxides the orbital ordering also accounts for opening of insulating band gap between the e_g $d(x^2-y^2)$ and $d(z^2)$ states of $\sim$1 eV and for large energy stabilization of the orbital-ordered structure in respect to the undistorted cubic one ($\Delta E_{PdO} = -2.271$ eV and $\Delta E_{PtO} = -1.497$ eV [18]). The energetic stabilization decreases with the increasing electron number as it is smaller for d^9 oxides ($\Delta E_{CuO} = -0.401$ eV, $\Delta E_{AgO} = -0.311$ eV), consistently with the weaker JT effect in these systems.

Magnetic ordering in CuO.—In CuO, the onset of the tetragonal $P4_2/mmc$ cell due to orbital ordering is suppressed by AFM interactions due to one unpaired electron on the Cu^{2+} cation. Simultaneously, they are responsible for stabilization of the phonon-induced monoclinic $C2/c$ cell and opening of the magnetic band gap (>2 eV, Fig. 4 right), while lowering the energy of the orbital-ordered structure by additional −0.514 eV. The magnetic pattern that couples to the soft mode L_3 in the cubic CuO lattice corresponds to orthorhombic $Pmmn$ ($Z=4$) symmetry. Such coupling results in a monoclinic $P2_1/c$ cell with $Z=8$, identical to the experimentally observed magnetic cell of CuO [19]. The group theory proves that the monoclinic $P2_1/c$ cell is a common subgroup of the $Pmmn$ and $C2/c$ ones: $C2/c(Z=2) \cap Pmmn(Z=4) \rightarrow P2_1/c(Z=8)$ (further details in Supplemental Material [13]).

Charge ordering in AgO.—In another d^9 monoxide, AgO, the AFM interactions compete with charge transfer $Ag^{2+}(d^9) \rightarrow Ag^{1+}(d^{10})/Ag^{3+}(d^8)$. While both mechanisms open a comparable electronic band gap of $\sim$1 eV the lowering of the energy due to charge transfer is larger (−0.137 eV in $P2_1/c$ and −0.131 eV in $I4_1/a$) than that due to the AFM interactions (−0.116 eV) [20]. The charge transfer is realized by coupling of both first-order (Ag^{3+}) and second-order (Ag^{1+}) JT distortions to the mode L_3 via two distinct charge-ordering (Ag^{1+}/Ag^{3+}) patterns. The first one is virtually equivalent to the spin up–spin down ordering exhibited in the AFM-II ($R\bar{3}m$) magnetic structure commonly observed in 3d monoxides and yields the experimentally observed monoclinic $P2_1/c$ ($Z=4$) structure of AgO. The second one is identical to the spin up–spin down ordering pattern seen for the AFM-IV ($Fd\bar{3}m$) structure and results in the second experimentally observed AgO form tetragonal $I4_1/a$ ($Z=8$). The two AgO structures, when viewed in their rock salt representations, differ only in stacking of the ab layers, in which the JT distortions take place [Fig. 2(a)]. In both cases, the insulating band gap opens between Ag^{1+} and Ag^{3+} e_g states of $d(x^2-y^2)$ symmetry highly hybridized with oxygen p bands (Fig. 4, right). The symmetry analysis based on the group theory confirmed that both experimentally observed AgO forms are related to the cubic $Fm\bar{3}m$ cell through the L_3 order parameter, each involving its different components.

Mercurophilic interactions in HgO.—In HgO, the imaginary mode L_3 leads us to two distinct dynamically stable monoclinic $C2/c$ structures with $Z=2$ and $Z=4$ accompanied by energy decrease of −0.249 and −0.227 eV, respectively. The two cells represent tetragonally and rhombohedrally distorted rock salt lattice, respectively. Structural analysis revealed that the small $C2/c$ cell is actually a superstructure ($1\times2\times1$) of the $Pnma$ type (with infinite zigzagged $[\text{Hg-O}]_\infty$ chains) and the large $C2/c$ one is equivalent to (a, b, $4c/3$) of the cinnabar structure (with helical $[\text{Hg-O}]_\infty$ chains; see Supplemental Material [13] for further details). Due to molecular nature of HgO, the stacking of the chains as well as the helical angle within the chains is governed by weak interactions. The closest attractive interchain contacts in HgO account for mercurophilic $Hg^{2+}\ldots Hg^{2+}$ bonds [21]. In the $Pnma$ form, they are found to be the weakest along the b vector. In consequence, various staking patterns along this vector may be stabilized as exemplified by the small $C2/c$ cell (the $1\times2\times1$ superstructure of $Pnma$) which is only 0.006 eV higher in energy. Additionally, it has been calculated previously [22], that the torsional potential related to the shape of the HgO chain is very flat with no minima between the helical angles 120°–180°. In consequence, helical chains with distinct periodicities may constitute local minima as exemplified by the big $C2/c$ cell with four atoms per helical chain in contrary to the three in $P3_121$ structure. This $1\times1\times4/3$ superstructure of $P3_121$ cell is energetically disfavored only by

0.021 eV and one can obtain the $P3_121$ structure from the $C2/c$ one simply by partially unscrewing the chain. The chain stacking as well as the helical angle has little impact on electronic band gap (~2.3–2.4 eV for all four cells), which further supports role of the weak interactions in crystal packing in HgO. In summary, the imaginary mode L_3 lead to polytopes build of parallel zigzagged and helical $[\text{Hg-O}]_\infty$ chains and thus to structures intimately related to the experimentally observed HgO forms.

In the above, we have provided a unified description of crystal structures of the LTM monoxides as emerging from the phonon-driven distortions of the rock salt lattice and their interplay with electronic degrees of freedom. On the basis of the hybrid DFT calculations and phonon direct method, we have shown that the experimentally observed LTM MO structures appear due the cooperative JT effects in the cubic $Fm\bar{3}m$ cell involving orbital ordering (PdO, PtO), coupled either to AFM interactions (CuO), to charge transfer (AgO), or to weak mercurophilic interactions (HgO $Pnma$ and $P3_121$). Most importantly, in all LTM MOs the relevant electronic degrees of freedom were all found to couple to the same order parameter—the doubly degenerate acoustic mode L_3 of the fcc structure. In the light of the presented results, one may conclude that all existing TM MOs (Fig. 1) crystallize either in the perfect or distorted forms of the rock salt structure, the distortion being either due to magnetic ordering (small distortion) or due to cooperative JT effect (large distortion). It turns out that the distortions in question lead to opening of the electronic band gap at the Fermi level of all LTM MOs studied. The propensity of the metallic state of rock salt lattice towards symmetry-breaking and electron-localizing lattice distortions is one characteristic feature of d^8, d^9, and certain d^{10} systems.

Calculation details.—DFT and hybrid DFT calculations for periodic systems were performed using the VASP package [23] within GGA approximation [24] and projector-augmented waves (PAW) [25], using PBEsol functional [26] and HSE06 hybrid one [27] (with HF/DFT mixing parameter $\alpha = 0.25$). Plane-wave cutoff of 520 eV and k-spacing of $0.35\,\text{Å}^{-1}$ (optimization and Hellmann-Feynman forces) and $0.2/0.25\ \text{Å}^{-1}$ (for single point energy and DOS calculations in DFT/hybrid DFT) was used. The DFT + U calculations [28] were performed for the spin-polarized AFM and nonmagnetic states of selected systems using broken-symmetry approach (see Supplemental Material [13]). The scalar relativistic effects are included in the potentials applied. The phonon dispersion curves for the $Fm\bar{3}m$ structures were obtained by the direct method implemented in PHONON [29] and using the Hellman-Feynman forces calculated for the $2 \times 2 \times 2$ supercells. Symmetry analysis was performed using codes COPL and ISOTROPHY [30]. All electronic band structure/DOS and phonon dispersion calculations were carried out for cells preoptimized at a given level of theory.

M. D. and W. G. acknowledge the Polish National Science Center (NCN), Grant No. UMO-2012/06/M/ST5/00344. P. P. acknowledges the Polish National Science Center (NCN), Grant No. UMO-2011/01/M/ST3/00738.

*mariana@icm.edu.pl

[1] J. Zaanen, G. A. Sawatzky, and J. W. Allen, Phys. Rev. Lett. **55**, 418 (1985).
[2] M. Imada, A. Fujimori, and Y. Tokura, Rev. Mod. Phys. **70**, 1039 (1998).
[3] W. L. Roth, Phys. Rev. **110**, 1333 (1958).
[4] W. Jauch, M. Reehuis, H. J. Bleif, F. Kubanek, and P. Pattison, Phys. Rev. B **64**, 052102 (2001).
[5] G. Tunell, E. Posnjak, and C. J. Ksanda, Z. Kristallogr. **90**, 120 (1935).
[6] W. J. Moore and L. Pauling, J. Am. Chem. Soc. **63**, 1392 (1941).
[7] J. A. McMillan, J. Inorg. Nucl. Chem. **13**, 28 (1960).
[8] K. Yvon, A. Bezinge, P. Tissot, and P. Fischer, J. Solid State Chem. **65**, 225 (1986).
[9] K. Aurivillius, Acta Chem. Scand. **18**, 1305 (1964).
[10] D. J. Benjamin, Mater. Res. Bull. **17**, 179 (1982). The $P\bar{1}$ cell is related to $Pnma$ by having a larger Hg-O-Hg intrachain angle which results in larger c of 7.01 Å (as compared to $a = 6.61$ Å in $Pnma$); a of $P\bar{1}$ corresponds to $2c$ of $Pnma$; thus $P\bar{1}$ was omitted from this study.
[11] K. Aurivillius and I. B. Carlsson, Acta Chem. Scand. **11**, 1069 (1957); K. Aurivillius and I. B. Carlsson, Acta Chem. Scand. **12**, 1297 (1958).
[12] M. Derzsi, A. Hermann, R. Hoffmann, and W. Grochala, Eur. J. Inorg. Chem. **29**, 5095 (2013).
[13] See Supplemental Material at http://link.aps.org/supplemental/10.1103/PhysRevLett.113.025505 for rock salt representations of LTM MOs and comparison of DFT, DFT+U and hybrid DFT results obtained in this study for the structural, electronic, magnetic and dynamic properties.
[14] NbO crystallizes in $Pm\bar{3}m$ cell—a rock salt lattice with 25% of vacancies. ZnO adopts wurtzite, and zinc blade type structures at ambient conditions but undergoes transition to the rock salt structure above 9 GPa: C. H. Bates, W. B. White, and R. Roy, Science **137**, 993 (1962).
[15] In the case of AgO the electronic ground state is properly reproduced only on hybrid DFT level: J. P. Allen, D. O. Scanlon, and G. W. Watson, Phys. Rev. B **81**, 161103(R) (2010). Therefore, in this case, the dispersion curves were recalculated on hybrid DFT level yielding the same results.
[16] For all structures, the electronic DOS was calculated on both DFT and hybrid DFT level. Although quantitatively comparable results were obtained on both levels for the cubic undistorted structures, implementation of hybrid functional turned out to be crucial for reproduction of the electronic structure in the vicinity of the Fermi level, opening of the band gap in the distorted structures and stabilization of charge-transfer mechanism in AgO.
[17] Throughout the document Z is defined as number of [MO] units per primitive cell.

[18] All energies in the text are listed per formula unit and are calculated on hybrid DFT level.
[19] B. Forsytht, P. J. Brown, and B. M. Wanklyn, J. Phys. C **21**, 2917 (1988); B. X. Yang, T. R. Thurston, J. M. Tranquada, and G. Shirane, Phys. Rev. B **39**, 4343 (1989); P. J. Brown, T. Chattopadhyay, J. B. Forsyth, and V. Nunez, J. Phys. Condens. Matter **3**, 4281 (1991).
[20] Two AFM models, CuO $P2_1/c$-type and AFM-II type, were considered. The latter one led to nonmagnetic solution since it prevents the orbital ordering, while forcing the magnetic moment due to the one unpaired electron to be smeared over both e_g orbitals.
[21] See Table S7 in ESM for analysis of Hg…Hg distances in HgO, and for details of mercurophilic interactions see D. M. Kumar and S. Dalela, Int. J. Mat. Phys., **4**, 11 (2013).
[22] C. X. Cui and M. Kertesz, Inorg. Chem. **29**, 2568 (1990).
[23] G. Kresse and J. Furthmüller, Comput. Mater. Sci. **6**, 15 (1996); G. Kresse and J. Furthmüller, Phys. Rev. B **54**, 11169 (1996).
[24] J. P. Perdew, K. Burke, and M. Ernzerhof, Phys. Rev. Lett. **77**, 3865 (1996).
[25] P. E. Blöchl, Phys. Rev. B **50**, 17953 (1994); G. Kresse and D. Joubert, Phys. Rev. B **59**, 1758 (1999).
[26] J. P. Perdew, A. Ruzsinszky, G. I. Csonka, O. A. Vydrov, G. E. Scuseria, L. A. Constantin, X. Zhou, and K. Burke, Phys. Rev. Lett. **100**, 136406 (2008).
[27] G. Kresse and J. Furthmüller, Comput. Mater. Sci. **6**, 15 (1996); G. Kresse and J. Furthmüller, Phys. Rev. B **54**, 11169 (1996).
[28] A. I. Liechtenstein, V. I. Anisimov, and J. Zaanen, Phys. Rev. B **52**, R5467 (1995).
[29] K. Parlinski, Z.- Q. Li, and Y. Kawazoe, Phys. Rev. Lett. **78**, 4063 (1997); K. Parlinski, Phonon Software, Kraków, 2011.
[30] ISOTROPHY Software Suite, http://iso.byu.edu.